# Cooperative folding of linear poly(dimethyl siloxane)s via supramolecular interactions

Macromolecular Rapid Communications
www.mrc-journal.de

# Cooperative Folding of Linear Poly(dimethyl siloxane)s via Supramolecular Interactions

*Marcin L. Ślęczkowski, E. W. Meijer,* and Anja R. A. Palmans**

**The synthesis and characterization of graft copolymers are reported based on linear poly(dimethyl siloxane) (PDMS) and chiral, pendant benzene-1,3,5-tricarboxamides (BTAs). The copolymers differ in degree of polymerization (DP) and BTA graft density. Characterization of the bulk materials at room temperature reveals that the BTAs aggregate in a helical fashion via threefold hydrogen-bond formation within the PDMS matrix. A significant degree of hydrogen bonding persists up to 180 °C, regardless of DP and BTA content. Analysis of the solution behavior by $^1$H NMR spectroscopy indicates that BTA aggregation occurs in $CDCl_3$, a solvent normally suppressing aggregation. Circular dichroism (CD) spectroscopy in 1,2-dichloroethane shows strong CD effects and reveals that increasing the DP and decreasing the BTA graft density results in an increase in the cooperativity of the BTA aggregation. Dynamic light scattering indicates the formation of particles with sizes of 400 nm. This is the first time that polymers with pendant BTAs show a sharp transition between a nonaggregated and aggregated state, a behavior similar to the one observed for "free" BTAs. The cooperative aggregation is attributed to the strong phase-segregation between the PDMS backbone and the BTAs, in combination with a high propensity of these polymers to form multichain aggregates.**

## 1. Introduction

Poly(dimethyl siloxane)s (PDMS) are a highly interesting and versatile class of polymers.[1–3] Their simple chemistry combined with the propensity to phase segregate[4] as well as the unique flexibility of the siloxane backbone[5–7] provides outstanding possibilities in the bottom-up synthesis of functional materials that found applications in microfluidic devices,[8] actuators,[9] as dielectric insulators in electronic devices.[10] Their biocompatibility with human tissue[11] and living cells[12] can potentially extend the applications toward biomaterials. Previous studies showed that strong phase-segregation is a powerful force that can drive the self-assembly of (macro)molecules in the bulk phase. Covalent block copolymers of poly(dimethyl siloxane) and poly(ethylene oxide),[13,14] poly(lactic acid),[15–17] poly(methacrylate),[18] poly(styrene),[19–21] and poly(2-vinylpyridine)[22] phase segregate to form well-ordered morphologies in the bulk. In addition, oligo- and poly(dimethyl siloxanes) have been combined with supramolecular hydrogen-bonding motifs to afford supramolecular block copolymers,[23] thermoplastic elastomers,[24,25] self-healing elastomers[26,27] and liquid crystalline materials.[28] The introduction of functionality in supramolecular phase segregating systems has been achieved by direct symmetrical end-functionalization of oligo(dimethyl siloxane) (oDMS) of discrete lengths with ureidopyrimidinone (UPy) units that are able to dimerize via fourfold hydrogen bond formation.[29] Protected UPy-oDMS conjugates exhibited liquid crystalline properties whereas deprotection caused a sharp transition toward block copolymer-like behavior.

In recent years, we and others have evaluated in detail the folding of single polymer chains driven by pendant hydrogen-bonding units in water[30–35] and organic media.[36–43] Notably, benzene-1,3,5-tricarboxamides (BTAs) have been found to efficiently fold polymers chains into compartmentalized structures in water. In organic media, in contrast, there is a propensity for multichain aggregation when dynamic hydrogen-bonding motifs are applied.[35] Often, these studies used poly(methacrylate)- or poly(norbornene)-based backbones in poor solvents, in which the conformational flexibility of the polymer backbone is reduced. We wondered in how far the high flexibility of the PDMS backbone, in combination with helical self-assembling BTAs, could enhance effective chain folding in organic media. In addition, we previously established that the folding of polymers with BTA pendants is noncooperative,[23,36] which is in stark contrast to the highly cooperative nature of the self-assembly of free BTAs.[44] The origin of the noncooperative behavior was attributed to the formation of several domains in which BTAs were aggregated within one polymer particle. This lack of ability of all BTAs to aggregate into one helical stack was associated with the high entropic penalty of the polymeric backbone to fold around a BTA stack.[30] The entropic penalty of the folding of the polymeric backbone offsets the normal cooperative behavior of BTAs, which has an enthalpic origin. The use of a highly flexible backbone, in contrast, could result in cooperative folding of the polymer chains.

M. L. Ślęczkowski, Prof. E. W. Meijer, Dr. A. R. A. Palmans
Laboratory of Macromolecular and Organic Chemistry
Institute for Complex Molecular Systems
Eindhoven University of Technology
P.O. Box 513, 5600 MB Eindhoven, The Netherlands
E-mail: e.w.meijer@tue.nl; a.palmans@tue.nl

The ORCID identification number(s) for the author(s) of this article can be found under https://doi.org/10.1002/marc.201700566.

**DOI: 10.1002/marc.201700566**

 

Inspired by the work of Bouteiller and co-workers,[45] we here decorate a PDMS backbone with BTA units affording graft polymers, encoded as **PDMS-*g*-BTA**. We vary the polymer length and BTA density along the backbone. The materials obtained are studied in detail in bulk using variable temperature infrared spectroscopy (VT-IR), circular dichroism (CD) spectroscopy, small angle X-ray scattering (SAXS), polarized optical microscopy (POM), and differential scanning calorimetry (DSC), whereas in dilute solution CD and dynamic light scattering (DLS) are used. Here, we show that strong phase segregation between the BTAs and the PDMS backbone in solution results in unparalleled cooperativity in the folding of the polymers, but at the same time also in the formation of large particles.

## 2. Results and Discussion

The synthesis of **PDMS-*g*-BTA** polymers (**Figure 1**A) required two building blocks, namely poly(dimethyl siloxane-*co*-methylhydrosiloxane) (**PDMS-*co*-PHMS**) copolymers and a BTA-olefin. **PDMS-*co*-PHMS** is commercially available with different average degrees of polymerization and molar PHMS content, which determines the degree of functionalization. The enantiomerically pure (*S*)-BTA-olefin has been synthesized in three steps via a parallel synthesis with good yield (29%) and high purity starting from trimesic acid according to the synthetic route shown in Schemes S1 and S2 in the Supporting Information.

**PDMS-*g*-BTA** was synthesized via direct hydrosilylation of three commercially available **PDMS-*co*-PHMS** with average molecular weights of 25 kg mol$^{-1}$ (5% PHMS), 6 kg mol$^{-1}$ (8% PHMS), and 2 kg mol$^{-1}$ (16% PHMS). The BTA olefin was coupled to the three polymers applying a platinum(0)-1,3-divinyl-1,1,3,3-tetramethyldisiloxane complex (the Karstedt catalyst). All polymers were purified by means of BioBeads in tetrahydrofuran (THF), which afforded a good separation between final product and the residual BTA-olefin impurities. The three polymers were fully characterized by $^1$H NMR and size exclusion chromatography (SEC) in THF (Figures S1–S3, Supporting Information). The results are summarized in **Table 1**.

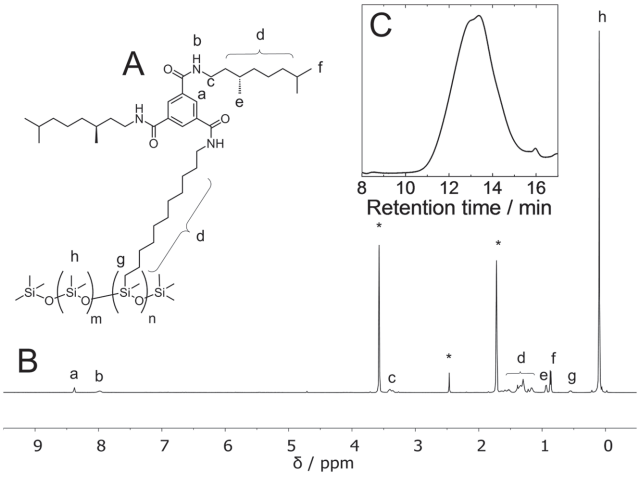


**Figure 1.** A) Chemical structure of **PDMS-*g*-BTA**. B) $^1$H NMR spectrum of **P1-*g*-BTA** in THF-$d_8$. * Peaks at 1.73 and 3.57 correspond to THF; peak at 2.46 ppm corresponds to water. C) SEC trace of **P1-*g*-BTA** in THF.

**Table 1.** Characterization data of polymers **PDMS-*g*-BTA**.

| Polymer | $M_n$[a] [kg mol$^{-1}$] | $Đ$[a] | mol% BTA[b] | $n$[c] | $m$[d] | $g$[e] |
|---|---|---|---|---|---|---|
| **P1-*g*-BTA** | 42.1 | 2.05 | 3 | 439 | 14 | −0.0012 |
| **P2-*g*-BTA** | 17.6 | 1.66 | 9 | 123 | 12 | −0.0019 |
| **P3-*g*-BTA** | 10.7 | 3.08 | 14 | 57 | 9 | −0.0023 |

[a]Determined by SEC in THF, calibrated with polystyrene standards; [b]Determined by $^1$H NMR; [c]$n$ is the number of siloxane units within the polymer backbone, which was calculated using the methylhydro siloxane content provided by the supplier and $M_n$; [d]$m$ is the number of BTA units within the polymer backbone, which was calculated using $M_n$ and mol% BTA; [e]The anisotropy value $g$ was determined from a film spin-coated on a quartz substrate.

As an illustrative example, the $^1$H NMR (THF-$d_8$) and SEC trace (THF) of **P1-*g*-BTA** are shown in Figure 1B,C. The $^1$H NMR spectrum of **P1-*g*-BTA** in THF-$d_8$ reveals the characteristic signals of the BTA core at 8.38 (Ph-H) and 7.98 ppm (NH) as well as the aliphatic protons (between 3.40 and 0.80 ppm). The largest peak at 0.10 ppm corresponds to the PDMS methyl protons. The BTA functionalization of PDMS is unambiguously confirmed by presence of a triplet at 0.5 ppm which corresponds to the methylene group attached to the PDMS backbone. The degree of BTA functionalization was quantified by comparing the integrals of the signals at 0.1 and 0.5 ppm (see the Supporting Information for details). For **P1-*g*-BTA** this results in a BTA graft density of 3%. **P2-*g*-BTA** and **P3-*g*-BTA** show higher graft densities of 9% and 14%, respectively (Table 1).

The SEC trace of **P1-*g*-BTA** in THF (Figure 1C) shows a unimodal peak, corresponding to an $M_n$ of 42.1 kg mol$^{-1}$ and a molar mass dispersity $Đ$ of 2.05. The measured $M_n$ is higher than expected (38 kg mol$^{-1}$ based on the SEC data of **PDMS-*co*-PHMS** and calculated degree of functionalization), presumably a result of the graft polymer topology in combination with the fact that the SEC column is calibrated with polystyrene standards. Analogously, **P2-*g*-BTA** and **P3-*g*-BTA** show also higher than expected values for $M_n$.

Interestingly, the differences in $M_n$ and BTA graft density are directly reflected in the physical appearance of the copolymers: whereas **P1-*g*-BTA** ($M_n$ = 42.1 kg mol$^{-1}$, 3 mol% BTAs) is a flexible solid, **P2-*g*-BTA** ($M_n$ = 17.6 kg mol$^{-1}$, 9 mol% BTAs) and **P3-*g*-BTA** ($M_n$ = 10.7 kg mol$^{-1}$, 14 mol% BTAs) are relatively hard and brittle materials. To investigate how the number of BTA grafts in combination with the degree of polymerization (DP) affects the bulk material properties, we performed Fourier-transform infrared spectroscopy (FT-IR), CD spectroscopy, DSC, SAXS, and POM studies. In the FT-IR spectrum of **P1-*g*-BTA** (**Figure 2**A) absorptions bands characteristic for helically aggregated BTAs[46] at 3238, 1641, and 1562 cm$^{-1}$ are observed as well as bands corresponding to the siloxane backbone (1250, 1010, and 790 cm$^{-1}$).[47] Bands at similar positions were found for **P2-*g*-BTA** and **P3-*g*-BTA** (Figures S4 and S5, Supporting Information), indicating that irrespective of the physical appearance of the polymers, helically aggregated BTAs are present in the

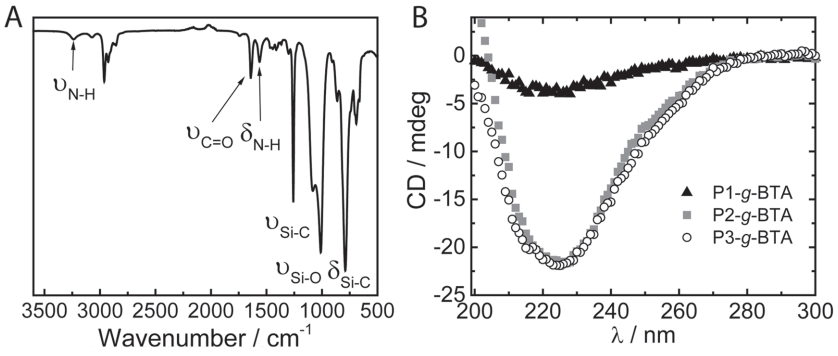


**Figure 2.** A) FT-IR spectrum of **P1-*g*-BTA**. B) CD spectra of spin-coated **PDMS-*g*-BTA** polymers; anisotropy values are given in Table 1.

bulk samples. This helical aggregation was further confirmed with CD spectroscopy. Since the chiral BTA grafts all possess (*S*)-stereogenic centra, we expect that an *M*-helical sense is favored in the formed aggregates, which is characterized by a negative CD effect.[48] Films of all polymers were spin coated on quartz and all **PDMS-*g*-BTA** polymers exhibited a negative CD effect with an extremum at 225 nm (Figure 2B). The anisotropy value (*g*) was calculated (Table 1) and the absolute values increase in the series **P1-*g*-BTA** to **P3-*g*-BTA**. This suggests that although helical aggregation is present in all graft copolymers, the degree to which this occurs depends on the density of the BTA grafts.

To further unravel the mesoscopic organization of **PDMS-*g*-BTA**, POM and SAXS measurements were performed. Under crossed polarizers, birefringence was observed in all samples (Figure S6, Supporting Information). However, the undefined textures indicate a poorly ordered structure. This lack of long range order was confirmed by the SAXS profile in which only small, broad peaks were visible in the low $q$ region (Figure S7, Supporting Information).

The stability of the BTA aggregates of **PDMS-*g*-BTA** polymers in bulk was studied using POM, DSC, and VT-IR. POM showed the loss of long-range order in the bulk materials starting at 150 °C for **P1-*g*-BTA** and **P2-*g*-BTA** and at 180 °C for **P3-*g*-BTA**. However, the loss of the birefringence was not connected to a loss of hydrogen bonds, as no visible transitions between −50 and 200 °C were observed in the DSC experiments. VT-IR of the **PDMS-*g*-BTA** series confirmed the observations from DSC since no substantial changes in the IR spectra were observed up to the temperatures at which the birefringence of samples was lost (Figures S8–S10, Supporting Information). In the N—H stretching region only a small shift from 3236 cm$^{-1}$ at room temperature to 3250 cm$^{-1}$ at 150 °C was observed, suggesting weakening of the strength of the hydrogen-bonded N—H stretch vibration. The carbonyl stretching absorption band remained unaffected whereas the behavior in the amide II region, which is a combination of different modes of vibration, is more complex. These results imply that the loss of birefringence under crossed polarizers is not connected to the loss of hydrogen bonding stabilizing the BTA aggregates, but rather is an outcome of decrease of viscosity within PDMS matrix. When the viscosity of PDMS decreases, the BTA aggregates become more mobile within the PDMS matrix, resulting in a loss of birefringence. From the above, we conclude that the BTA grafts attached covalently to the PDMS backbone form stable crosslinks stabilized by threefold hydrogen bonds in the bulk at room temperature. Increasing the temperature up to 180 °C results in weakening of the hydrogen bonds, but significant hydrogen bonding remains present, regardless of the degree of polymerization and BTA content.

We continued by investigating the effect of solvent on BTA-grafts association in **PDMS-*g*-BTA** systems. Previous studies of BTA-grafted polymers showed that these can form globular particles comprising single polymer chains in organic solvents and water via self-assembly of the BTAs followed by polymeric chain folding. However, the interplay between the backbone solubility in the solvent and BTA aggregation can also result in multichain aggregation and since the PDMS backbone is exceptionally flexible, the question is in how far this promotes or impedes single chain folding.

All three **PDMS-*g*-BTA** polymers give well-structured and sharp $^1$H NMR spectra in THF-$d_8$, indicating a lack of interactions between BTAs (Figure 1A). In contrast, the spectra of **PDMS-*g*-BTA** polymers in $CDCl_3$ (Figures S11–S13, Supporting Information) give broadened peaks with reduced intensities, indicative of aggregation. This is a striking difference in comparison to the behavior of the individual components, PDMS and BTA, which both show sharp signals in chloroform. Dilute solution characterization of **PDMS-*g*-BTA** was performed with CD spectroscopy. For this, 1,2-dichloroethane (DCE), which has a better optical transparency in the BTA absorption region than chloroform, was selected. In contrast to "free BTA" molecules that do not aggregate in chloroform and DCE, **PDMS-*g*-BTA** solutions in DCE ($c_{BTA}$ = 50 μm) all showed negative CD effects with extrema at 225 nm (**Figure 3**A). Interestingly, and in sharp contrast to the CD spectra in bulk, the molar circular dichroism ($|\Delta\varepsilon|$) of **P1-*g*-BTA** is now the highest of the three polymers ($|\Delta\varepsilon|$ = 43, 20, and 22 L mol$^{-1}$ for **P1-*g*-BTA**, **P2-*g*-BTA**, and **P3-*g*-BTA**, respectively). This remarkable difference highlights the importance of BTA-solvent and PDMS-solvent interactions which promote the aggregation of BTAs to the magnitude of "free BTA" in heptane ($|\Delta\varepsilon|$ = 43 L mol$^{-1}$ for "free BTA" in heptane)[44] and significantly larger than those observed for polymethacrylate (PMA)-BTA polymers.[37,38,43] This indicates that nearly all BTAs in **P1-*g*-BTA** are present in helical aggregates. On the other hand, values of $|\Delta\varepsilon|$ for **P2-*g*-BTA** and **P3-*g*-BTA** are close to the ones reported for PMMA-BTA polymers.[37,38,43] This suggests that a number of BTA units does not participate in helical assemblies in **P2-*g*-BTA** and **P3-*g*-BTA** whereas nearly all BTAs do in **P1-*g*-BTA**. Possibly, the higher local concentration of the BTA pendants in **P2-*g*-BTA** and **P3-*g*-BTA** reduces the conformational freedom of the polymers, preventing remaining BTAs to aggregate as effectively as in the case of **P1-*g*-BTA**.

Temperature-dependent CD measurements were conducted by cooling the dilute solutions of **PDMS-*g*-BTA** from 100 to 0 °C (Figure 3B). At 90 °C, no CD effect is visible, indicating that the BTAs are not aggregated. Upon cooling, an abrupt increase in the CD effect is observed for **P1-*g*-BTA** at 72 °C, a less abrupt increase takes place in case of **P2-*g*-BTA** at 70 °C, and **P3-*g*-BTA**

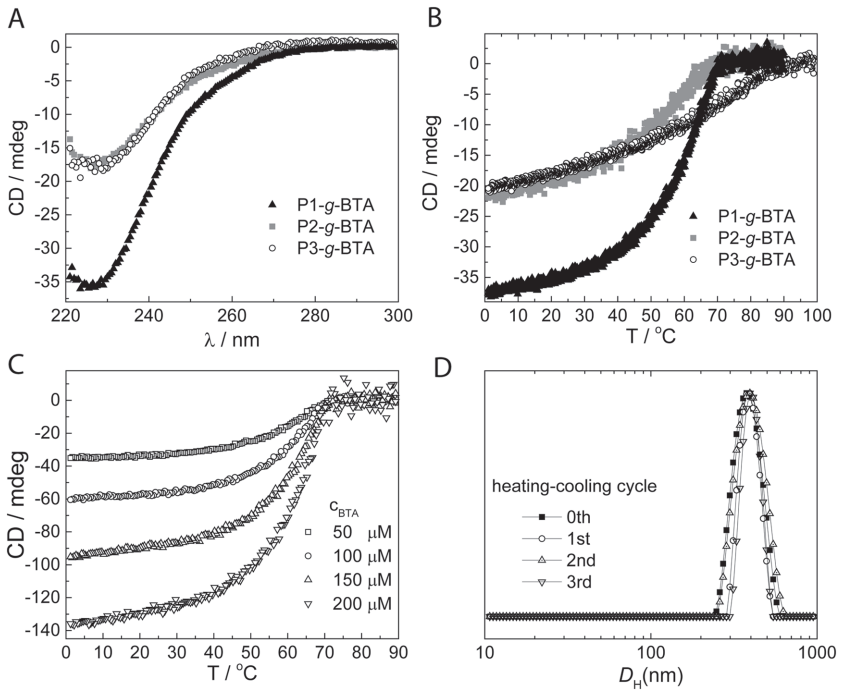


**Figure 3.** A) Full CD spectra of **PDMS-*g*-BTA** in DCE. $c_{BTA} = 50 \times 10^{-6}$ M, optical path length = 0.5 cm, $T = 20$ °C. B) CD cooling curves of **PDMS-*g*-BTA** series recorded at $\lambda = 227$ nm in DCE (cooling rate = 1 K min$^{-1}$). $c_{BTA} = 50 \times 10^{-6}$ M, optical path length = 0.5 cm. C) CD cooling curves of **P1-*g*-BTA** recorded at different concentrations, $\lambda = 227$ nm in DCE (cooling rate = 1 K min$^{-1}$), optical path length = 0.5 cm. D) DLS profiles of **P1-*g*-BTA** in DCE at 1 mg mL$^{-1}$ and 20 °C after heating–cooling cycles in the temperature interval of 20–75 °C.

exhibits a cooling curve similar to previously reported for carbon-based polymers with BTA pendants, which all exhibited a gradual increase of the CD effect.[30,31,35,37,38,49] The shapes of the cooling curves are connected to the increase of the density of BTA pendants. Despite the differences in the sharpness of the transition between **P2-*g*-BTA** and **P3-*g*-BTA**, the values of $|\Delta\varepsilon|$ are similar. **P1-*g*-BTA** shows a cooling curve similar to the ones recorded for free BTAs in alkane solvents, which is indicative for highly cooperative BTA aggregation.[44] As the degree of functionalization is increased, the sharpness in the transition, and therefore the cooperativity, diminishes. In addition, increasing the BTA concentration of **P1-*g*-BTA** from 50 to 200 μM shows that the $T_e$ remains at around 72 °C, the CD effect increases proportionally with the BTA concentration, and that the cooperativity of the transition remains very high (Figure 3C).

DLS experiments performed on **P1-*g*-BTA** in DCE at 20 °C show the presence of particles with sizes of around 400 nm hydrodynamic diameter with a low dispersity (Figure 3D). This clearly indicates that large particles are formed in DCE. Interestingly, the size of the formed particles at room temperature remains unaffected after heating–cooling cycles (Figure 3D), indicating that the formation of the particles is thermodynamically controlled.

Based on the results above, we propose that the remarkable cooperative BTA aggregation observed in **P1-*g*-BTA** is related to the highly incompatible nature of PDMS and the covalently attached BTAs combined with the formation of helical BTA aggregates. In addition to the phase-segregation process, there is also the intrinsic flexibility of the PDMS backbone[4,7] which significantly reduces the entropic penalty of backbone folding in comparison to the more stiff PMMA backbones, permitting a high degree of aggregation between pendant BTAs. Also, the poor solubility of PDMS in DCE at lower temperatures could play an important role. At room temperature, the mixture of the pure precursor polymer **PDMS-*co*-PHMS** in DCE is turbid at 10 mg mL$^{-1}$ whereas the mixture becomes clear when heated above 50 °C. Covalently attaching the BTAs changes the solvent compatibility of the graft copolymer. At the same time, the PDMS backbone may shield the BTAs from the solvent, hereby enhancing hydrogen-bonding interactions. Although it appears from the above results that the collapse of the PDMS backbone in DCE creates a confined space that promotes BTA aggregation, the exact nature of the interaction triangle between DCE, BTA, and PDMS is not fully clear and is topic of further investigations.

## 3. Conclusions

We have shown that supramolecular assembly of BTAs attached to PDMS leads to phase segregated structures in bulk. The formation of helical aggregates stabilized by threefold hydrogen bonding was confirmed by IR and CD spectroscopy. The formed superstructures were stable up to 180 °C. In addition, we demonstrated that proper selection of the polymeric backbone can lead to extraordinary folding properties. **P1-*g*-BTA** exhibited highly cooperative assembly of the BTAs in DCE, which was not achieved for any BTA-graft copolymers before and suggests that this unusual behavior is connected to the synergy between BTA-backbone, BTA-solvent, and backbone-solvent interactions. This combination leads to the thermodynamically controlled formation of multichain aggregates in which nearly all BTAs are aggregated. The degree of functionalization in combination with the degree of polymerization also has a significant impact on the folding characteristics, which indicates that a proper balance in BTA density is needed. An important question is how sequence and dispersity control will affect the cooperative folding behavior of **PDMS-*g*-BTA** and further studies will be devoted to this topic.

## Supporting Information

Supporting Information is available from the Wiley Online Library or from the author.

## Acknowledgements

The authors would like to thank Bas van Genabeek for performing the SAXS measurements. This work was financed by European Union's

 

Horizon 2020 research and innovation program under the Marie Sklodowska-Curie grant agreement No 642083.

## Conflict of Interest

The authors declare no conflict of interest.

## Keywords

cooperativity, hydrogen bonding, phase-segregation, poly(dimethyl siloxane), supramolecular chemistry

Received: August 18, 2017
Revised: September 22, 2017
Published online: November 6, 2017

[1] D. Zhu, S. Handschuh-Wang, X. Zhou, *J. Mater. Chem. A* **2017**, *5*, 16467.
[2] J. Zhou, A. V. Ellis, N. H. Voelcker, *Electrophoresis* **2010**, *31*, 2.
[3] F. Abbasi, H. Mirzadeh, A. A. Katbab, *Polym. Int.* **2001**, *50*, 1279.
[4] E. Yilgör, I. Yilgör, *Prog. Polym. Sci.* **2014**, *39*, 1165.
[5] W. L. Roth, *J. Am. Chem. Soc.* **1947**, *69*, 274.
[6] E. L. Warrick, J. Hunter, A. J. Barr, *Ind. Eng. Chem.* **1952**, *44*, 2196.
[7] F. Weinhold, R. West, *Organometallics* **2011**, *30*, 5815.
[8] J. C. McDonald, D. C. Duffy, J. R. Anderson, D. T. Chiu, H. Wu, O. J. Schueller, G. M. Whitesides, *Electrophoresis* **2000**, *21*, 27.
[9] M. A. Unger, H. P. Chou, T. Thorsen, A. Scherer, S. R. Quake, *Science* **2000**, *288*, 113.
[10] J. Veres, S. D. Ogier, S. W. Leeming, D. C. Cupertino, S. M. Khaffaf, *Adv. Funct. Mater.* **2003**, *13*, 199.
[11] Y. Mi, Y. Chan, D. Trau, P. Huang, E. Chen, *Polymer* **2006**, *47*, 5124.
[12] N. Q. Balaban, U. S. Schwarz, D. Riveline, P. Goichberg, G. Tzur, I. Sabanay, D. Mahalu, S. Safran, A. Bershadsky, L. Addadi, B. Geiger, *Nat. Cell Biol.* **2001**, *3*, 466.
[13] M. Galin, A. Mathis, *Macromolecules* **1981**, *14*, 677.
[14] J. Yang, G. Wegner, R. Koningsveld, *Colloid Polym. Sci.* **1992**, *270*, 1080.
[15] L. M. Pitet, S. F. Wuister, E. Peeters, E. J. Kramer, C. J. Hawker, E. W. Meijer, *Macromolecules* **2013**, *46*, 8289.
[16] M. D. Rodwogin, C. S. Spanjers, C. Leighton, M. A. Hillmyer, *ACS Nano* **2010**, *4*, 725.
[17] B. van Genabeek, B. F. M. De Waal, M. M. J. Gosens, L. M. Pitet, A. R. A. Palmans, E. W. Meijer, *J. Am. Chem. Soc.* **2016**, *138*, 4210.
[18] Y. Luo, D. Montarnal, S. Kim, W. Shi, K. P. Barteau, C. W. Pester, P. D. Hustad, M. D. Christianson, G. H. Fredrickson, E. J. Kramer, C. J. Hawker, *Macromolecules* **2015**, *48*, 3422.
[19] Y. S. Jung, J. B. Chang, E. Verploegen, K. K. Berggren, C. A. Ross, *Nano Lett.* **2010**, *10*, 1000.
[20] Y. S. Jung, C. A. Ross, *Nano Lett.* **2007**, *7*, 2046.
[21] I. Bita, J. K. Yang, Y. S. Jung, C. A. Ross, E. L. Thomas, K. K. Berggren, *Science* **2008**, *321*, 939.
[22] J. W. Jeong, W. I. Park, M. J. Kim, C. A. Ross, Y. S. Jung, *Nano Lett.* **2011**, *11*, 4095.
[23] L. M. Pitet, A. H. M. van Loon, E. J. Kramer, C. J. Hawker, E. W. Meijer, *ACS Macro Lett.* **2013**, *2*, 1006.
[24] D. Tyagi, I. Yilgor, J. E. McGrath, G. L. Wilkes, *Polymer* **1984**, *25*, 1807.
[25] N. E. Botterhuis, D. J. M. van Beek, G. M. L. van Gemert, A. W. Bosman, R. P. Sijbesma, *J. Polym. Sci., Part A: Polym. Chem.* **2008**, *46*, 3877.
[26] J. Zhao, R. Xu, G. Luo, J. Wu, H. Xia, *Polym. Chem.* **2016**, *7*, 7278.
[27] C. H. Li, C. Wang, C. Keplinger, J. L. Zuo, L. Jin, Y. Sun, P. Zheng, Y. Cao, F. Lissel, C. Linder, X. Z. You, Z. Bao, *Nat. Chem.* **2016**, *8*, 618.
[28] M. García-Iglesias, B. F. M. de Waal, I. de Feijter, A. R. A. Palmans, E. W. Meijer, *Chemistry* **2015**, *21*, 377.
[29] R. H. Zha, B. F. M. De Waal, M. Lutz, A. J. P. Teunissen, E. W. Meijer, *J. Am. Chem. Soc.* **2016**, *138*, 5693.
[30] P. J. M. Stals, M. A. J. Gillissen, T. F. E. Paffen, T. F. A. De Greef, P. Lindner, E. W. Meijer, A. R. A. Palmans, I. K. Voets, *Macromolecules* **2014**, *47*, 2947.
[31] T. Terashima, T. Mes, T. F. A. De Greef, M. A. J. Gillissen, P. Besenius, A. R. A. Palmans, E. W. Meijer, *J. Am. Chem. Soc.* **2011**, *133*, 4742.
[32] G. M. ter Huurne, M. A. J. Gillissen, A. R. A. Palmans, I. K. Voets, E. W. Meijer, *Macromolecules* **2015**, *48*, 3949.
[33] M. A. J. Gillissen, T. Terashima, E. W. Meijer, A. R. A. Palmans, I. K. Voets, *Macromolecules* **2013**, *46*, 4120.
[34] M. Artar, T. Terashima, M. Sawamoto, E. W. Meijer, A. R. A. Palmans, *J. Polym. Sci., Part A: Polym. Chem.* **2014**, *52*, 12.
[35] E. Huerta, B. van Genabeek, P. J. M. Stals, E. W. Meijer, A. R. A. Palmans, *Macromol. Rapid Commun.* **2014**, *35*, 1320.
[36] O. Altintas, E. Lejeune, P. Gerstel, C. Barner-Kowollik, *Polym. Chem.* **2012**, *3*, 640.
[37] T. Mes, R. Van Der Weegen, A. R. A. Palmans, E. W. Meijer, *Angew. Chem., Int. Ed.* **2011**, *50*, 5085.
[38] E. W. Hosono, N. Gillissen, M. A. J. Li, Y. Scheiko, S. S. Palmans, A. R. A. Meijer, *J. Am. Chem. Soc.* **2012**, *135*, 501.
[39] O. Altintas, T. Rudolph, C. Barner-Kowollik, *J. Polym. Sci., Part A: Polym. Chem.* **2011**, *49*, 2566.
[40] E. J. Foster, E. B. Berda, E. W. Meijer, *J. Am. Chem. Soc.* **2009**, *131*, 6964.
[41] P. J. M. Stals, M. A. J. Gillissen, R. Nicolaÿ, A. R. A. Palmans, E. W. Meijer, *Polym. Chem.* **2013**, *4*, 2584.
[42] O. Altintas, M. Artar, G. ter Huurne, I. K. Voets, A. R. A. Palmans, C. Barner-Kowollik, E. W. Meijer, *Macromolecules* **2015**, *48*, 8921.
[43] Y. Ogura, M. Artar, A. R. A. Palmans, M. Sawamoto, E. W. Meijer, T. Terashima, *Macromolecules* **2017**, *50*, 3215.
[44] M. M. J. Smulders, A. P. H. J. Schenning, E. W. Meijer, *J. Am. Chem. Soc.* **2008**, *130*, 606.
[45] O. Colombani, C. Barioz, L. Bouteiller, C. Chanéac, L. Fompérie, F. Lortie, H. Montès, *Macromolecules* **2005**, *38*, 1752.
[46] P. J. M. Stals, M. M. J. Smulders, R. Martín-Rapún, A. R. A. Palmans, E. W. Meijer, *Chem. Eur. J.* **2009**, *15*, 2071.
[47] M. A. Obrezkova, A. A. Kalinina, I. V. Pavlichenko, N. G. Vasilenko, M. V. Mironova, A. V. Semakov, V. G. Kulichikhin, M. I. Buzin, A. M. Muzafarov, *Silicon* **2014**, *7*, 177.
[48] L. Brunsveld, A. P. H. J. Schenning, M. A. C. Broeren, H. M. Janssen, J. A. J. M. Vekemans, E. W. Meijer, *Chem. Lett.* **2000**, *29*, 292.
[49] N. Hosono, A. R. A. Palmans, E. W. Meijer, *Chem. Commun.* **2014**, *50*, 7990.

 